Nuclear specific heat of bcc ^{3}He near the magnetic ordering transitions

Dennis S. Greywall and Paul A. Busch
AT&T Bell Laboratories, Murray Hill, New Jersey 07974
(Received 3 April 1987)

Precise specific-heat measurements were made on low-density samples of bcc ^{3}He in the vicinity of the various magnetic ordering transitions. The data obtained for magnetic fields of 0, 6, and 10 kOe span the temperature range 0.6–10 mK. At $H=0$, the data exhibit an extremely sharp peak indicative of a first-order transition. Below T_N the specific heat is proportional to T^3 and yields a spin-wave velocity ($v_{\rm spin}$) in excellent agreement with a previous determination. Above T_N, the results show no anomalous satellite peaks as seen in other experiments and as suggested by theoretical calculations. Within the precision of the measurements, the effect of changing the density is only to rescale the temperature. The data obtained at 6 and 10 kOe, when plotted as a function of T/T_c, nearly fall on a universal curve with a shape characteristic of a λ-type transition. A detailed analysis of the density distribution in the solid ^{3}He samples supports the claim that this transition is second order. At 10 kOe, T_c is found to be proportional to $V^{8.7}$, where V is the molar volume. It is demonstrated, however, that this dependence is consistent with the exchange energies being proportional to V^{17}, in agreement with other experiments. As a function of increasing field, $v_{\rm spin}$ decreases for $H<4$ kOe and increases at higher fields. Above 4 kOe, $v_{\rm spin}$ is proportional to T_c. The field-induced increase in the paramagnetic-phase specific heat can be described well by the free-spin expression with an effective magnetic moment equal to $0.83\mu_B$. Magnetization results inferred from the specific-heat data are in excellent agreement with direct measurements. The H-T phase diagram which is thermodynamically consistent with the new data is presented. Also included are results for the field-dependent boundary resistance between solid ^{3}He and silver.

I. INTRODUCTION

The thermodynamic properties of solid ^{3}He at millikelvin temperatures are completely dominated by the contribution from the nuclear-spin ($\frac{1}{2}$) system.[1,2] This implies spin interactions which are several orders of magnitude larger than the direct dipole-dipole term. The overpowering effective interaction is a consequence of atom-atom exchange which is non-negligible in the low-density solid due to the very large zero-point motion of the ^{3}He atoms about their average locations in the bcc lattice. Exchange therefore also explains the extremely high nuclear-spin ordering temperature: roughly 1 mK (Ref. 3) in zero magnetic field. Another intriguing aspect of the spin ordering is the modification induced by a relatively weak applied magnetic field. The pioneering work in this area was done by Adams and co-workers[4] more than ten years ago. Their measurements demonstrated the existence of boundaries in the H-T phase diagram which separate the plane into three distinct regions. Although there has been significant subsequent progress, both experimentally and theoretically, the three "phases" are still not completely understood; in fact, several quite fundamental issues remain unresolved.

In this paper we add to the data base for solid ^{3}He by presenting the results of high-precision specific-heat measurements, performed in the vicinity of the various magnetic ordering transitions. In addition to demonstrating the order of the transitions, the data give information about the elementary excitations in the ordered phases. At somewhat higher temperatures the results show the significant departures from the limiting high-temperature behavior. The new results are compared in detail with other thermodynamic measurements. We demonstrate, in particular, thermodynamic consistency with previous magnetization results. The implications in regard to the H-T phase diagram are also discussed.

II. EXPERIMENTAL DETAILS

A. Calorimeter

A cross-sectional drawing of the calorimeter is shown in Fig. 1. It is comprised of three major components: the sample cell, the LCMN (lanthanum-diluted cerium magnesium nitrate) thermometer chamber, and a physically small high-field superconducting solenoid which is thermally isolated from the cell. Thermal contact between the cell and the $PrNi_5$ cooling stage[5] is made via a superconducting tin heat switch. The cell and magnet are each rigidly positioned above the same flange using thermally insulating screws and spacers. This flange, in turn, is clamped to the cooling stage using a heavy post machined as part of the silver flange. The magnet is thermally connected to the mixing chamber of the dilution refrigerator with a copper bus.

The cell and thermometer chamber are made primarily of high-purity silver because of this material's high thermal conductivity and also because of its small nuclear heat capacity in a magnetic field. The annular sample chamber is centered at the midpoint of the magnet and is packed with 3.63 g of fine silver power[6] at

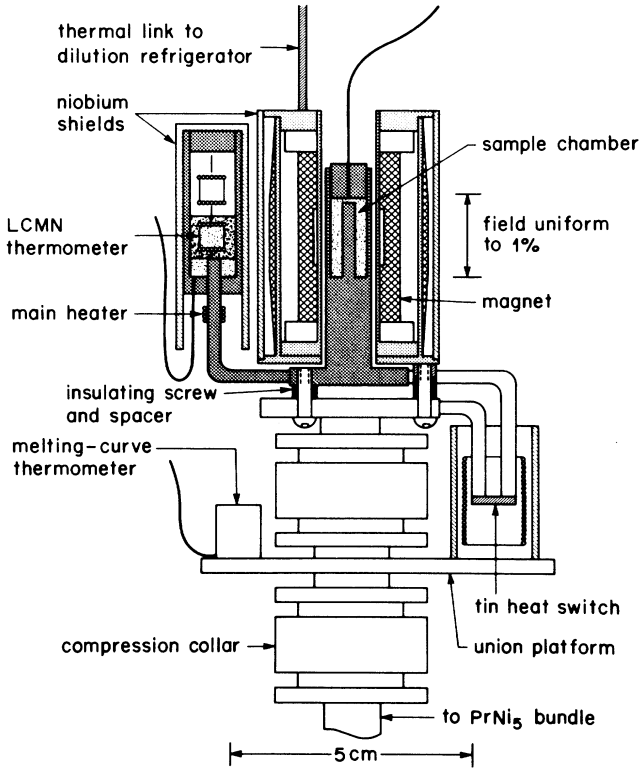

FIG. 1. Calorimeter.

42% of solid density. The i.d., o.d., and height of the cavity are 3.2, 8.3, and 17.8 mm, respectively. Because of the large specific heat and small thermal conductivity of solid ^{3}He at very low temperature, the sample is confined to the small pores in the silver sponge in order to obtain internal thermal relaxation times on the order of minutes near the ordering transitions. Having all of the sample in close proximity to the metal surface also serves to reduce the spin-lattice relaxation time. The central post passing through the sample chamber ensures good thermal contact between the cell body and the silver sponge even though there is a slight expansion of the annealed cell under pressurization. In an attempt to further improve the contact to the cell body, the silver powder was not sintered at elevated temperature because of the consequential shrinkage. Moreover, heating of the packed powder would have reduced its surface area. The total surface area in the cell is estimated[7] to be 10.5 m^2, which implies[8] an average pore diameter of about 2000 Å. Consequently, roughly 1% of the ^{3}He atoms are in direct contact with the metal surface. The total open volume of the cell is 0.45 cm^3.

The LCMN thermometer, Fig. 1, is housed in a separate chamber to isolate it from the magnetic field applied to the solid sample and to permit liquid ^{3}He to be used as the contact between the LCMN powder and the metal container. Compressed into the bottom portion of this chamber is 1.3 g of silver powder with a total surface area of 3.8 m^2. Roughly, 0.7 cm^3 of liquid ^{3}He completely submerges the lower coil, Fig. 1, containing the paramagnetic salt. The thermometer chamber is joined to the sample cell with a short length of 3.2-mm-diam silver rod, which is welded to the cell and hard-soldered to the thermometer chamber. Wound on this rod and near the thermometer is a 165-Ω Pt-W calorimeter heater. Both the thermometer and heater are covered by a niobium shield.

The superconducting magnet is patterned after others described in the literature.[9–11] It features a compensation coil counterwound concentric with the main coil which reduces the field to near zero at the radial position of the niobium shield. The i.d. of the solenoid is 11.7 mm and the field-to-current ratio is 1.95 kOe/A. Central uniformity of the field is better than 1% over a length of 1.8 cm. The coils are wound on copper mandrels using insulated 0.15-mm-diam copper-clad NbTi monofilament wire. The persistent switch for the magnet is located on the still of the dilution refrigerator.

Using a physically small magnet permits an extremely rigid mounting relative to the sample cell. This is important for reducing the amount of eddy-current heating of the calorimeter. It also makes it possible to have the susceptibility thermometer in close proximity to the sample cell. Moreover, problems associated with electrical leads passing into a high-field region are eliminated.

B. Thermometry

The self-inductance LCMN (5% CMN) thermometer is in most respects identical to the one described in Ref. 2. It was calibrated assuming the Curie-Weiss relation

$$\frac{1}{T-\Delta} = A\chi + B \ , \tag{1}$$

with A, B, and Δ adjustable parameters. These parameters were determined by measuring the susceptibility at three fixed points: $T_c^l(0)$, the superfluid transition temperature of liquid ^{3}He under vapor pressure; T_A, the superfluid transition of liquid ^{3}He on the melting curve; and T_W, the superconducting transition temperature[13] of tungsten. The transition at zero pressure was easily located by the kink in the warming curve observed with the sample chamber empty, but with liquid ^{3}He partially filling the thermometer chamber. The two higher-temperature calibration points were obtained (with the heat switch closed) by comparisons with a melting-curve thermometer,[14] see Fig. 1. Temperatures were assigned to these points, namely 0.93, 2.49, and 15.57 mK, based on the temperature scale presented in Ref. 12. The Weiss constant Δ for this thermometer was found to be -0.118 mK.

Before filling the sample cell with helium, determinations of the LCMN bridge ratio at T_c^l were made with the sample cell subjected to magnetic fields of 0,1,2, and 5 kOe. The high fields did not affect the thermometry; to within the precision of the measurements, all of these bridge ratio values were the same.

C. Specific-heat measurements

The heat-capacity data were obtained using the standard heat-pulse technique. A typical measurement in

zero applied field is shown in Fig. 2 for a temperature near 1.5 mK. Here the time needed to reestablish thermal equilibrium between the cell and sample following the heat pulse is of the order of minutes. However, at higher fields the relaxation time was much longer, as indicated by the dashed curves in the figure. The implied dramatic field dependence of the thermal boundary resistance is discussed in the Appendix. The relaxation time also increased with decreasing temperature. As a result only three or four heat-capacity measurements could be made per day near 1 mK and in a field of 10 kOe.

The number of moles of sample was computed using the cell volume and the molar-volume–versus–pressure relation given by Eq. (2) in Ref. 12. The cell volume was determined by the constraint that the measured molar entropy of the solid ^{3}He sample be R ln2 at high temperature. This volume differed by only 3% from that computed using the linear dimensions of the sample chamber and the mass of the silver powder.

D. Addendum heat capacity

The addendum contribution to the total measured heat capacity is due almost entirely to the liquid ^{3}He in the thermometer capsule. This quantity was measured with a precision of about 1% between 1 and 10 mK, before ^{3}He was admitted to the *sample* chamber. From the data obtained near 10 mK it was determined that the thermometer chamber contained 0.75 cm^3 of ^{3}He. The heat-capacity data at the higher temperatures are proportional to the temperature; however, as the temperature is decreased an excess contribution becomes progressively more significant. This excess was also observed in previous measurements of the heat capacity of liquid ^{3}He.[12,15] As in Ref. 12, this contribution could be adequately described by $Ae^{-T/B}$ with $B=1.0$ mK. In the present work $A=0.40$ mJ/K, whereas in Ref. 12 $A=1.0$. These two values scale accurately with the surface areas of the respective containers, but not with the masses of the silver powders which had undergone different heat treatments. The evidence is therefore that the excess is due to a surface effect and not to impurities in the sinter.

The addendum heat capacity was not measured below T_c^l. Because of its small size relative to the solid ^{3}He heat capacity, it was sufficient to approximate the bulk contribution as being proportional to T^3 with the coefficient adjusted to give the correct jump[12] at T_c^l.

Although the electronic heat capacity of the silver cell is completely negligible, the nuclear-spin contribution to the addendum in nonzero fields must be considered. This heat capacity is given by $C=\Lambda(H/T)^2$ with $\Lambda=1.38\times10^{-11}$ J K kOe^{-2} cm^{-3}. This relation implies that the heat capacity of silver (per cm^3) at $H=5$ kOe exceeds that of liquid ^{3}He below about 1 mK, and that of solid ^{3}He below a few tenths of a mK. The lowest temperature at which we made measurements is 0.6 mK, and here the silver contribution is several percent of the sample heat capacity. However, only a fraction of this contribution is actually probed by our measurements because of the very long spin-lattice relaxation time for silver. The Korringa constant is 11 s K, which implies a

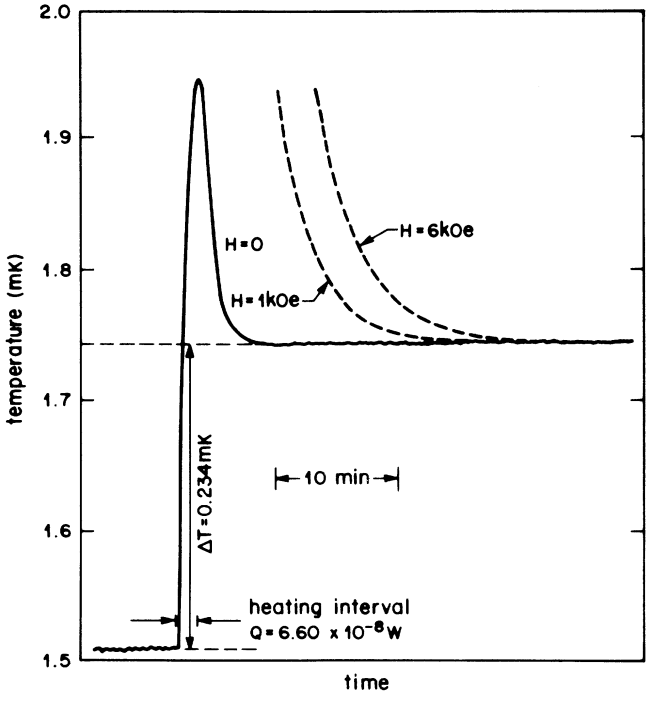

FIG. 2. Typical heat-capacity measurement in zero magnetic field. The dashed curves show the much longer relaxation times encountered at higher fields.

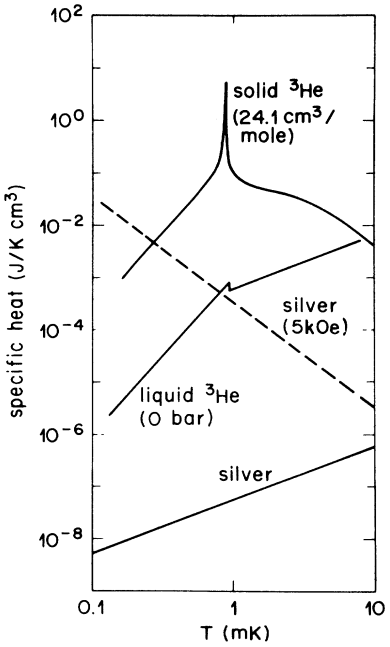

FIG. 3. Comparison of sample and addendum heat capacities.

TABLE I. Some parameters of the ^{3}He samples studied.

			$H=0$			$H=10$ kOe	
V (cm^3)	$\lvert J_{xx}\rvert/k_B$[a] (mK)	T_N (mK)	C/RT^3 (mK^{-3})	$v_{\text{spin}}^{\text{LFP}}$ (cm/s)	T_c (mK)	C/RT^3 (mK^{-3})	$v_{\text{spin}}^{\text{HFP}}$ (cm/s)
24.22	0.751	0.93[b]					
24.126	0.703	0.88	0.68	7.0	1.262	0.430	6.5
23.900	0.600	0.76	0.96	6.2	1.163	0.562	6.0
23.418	0.425				0.975		

[a]Based on Eq. (6).
[b]From Ref. 12.

relaxation time of 5 h at our lowest temperature. We deemed it unnecessary, therefore, to include in the addendum any contribution from the silver cell.

As Fig. 3 shows, near 10 mK, the addendum due to the liquid ^{3}He in the thermometer chamber is about equal to the heat capacity of the sample. It is mainly for this reason that the heat-capacity measurements were not extended to higher temperatures. We also note that above 10 mK the LCMN thermometer has little sensitivity and also a long thermal time constant.

III. RESULTS AND DISCUSSION

All of the specific-heat results on bcc ^{3}He presented in this paper were obtained in the vicinity of the various magnetic ordering transitions. The measurements were made at molar volumes of 24.13 and 23.90 cm^3, in fields of 0, 6, and 10 kOe and for temperatures in the range 0.6–10 mK. Above 1.5 mK the data have a precision of about 1%. Other numerical information for each of the samples is given in Table I.

The results at $H=0$, shown plotted on log-log scales in Figs. 4 and 5, show obvious qualitative differences from the 10-kOe data presented in Figs. 6 and 7. This reflects the crossing of a different phase boundary, Fig. 8. At $H=0$, the transition is from the low-field phase (LFP) to the paramagnetic phase (PP). At $H=10$ kOe the transition is from the high-field phase (HFP) to the paramagnetic phase. The LFP is believed to be antiferromagnetic with ferromagnetically aligned (100) planes in the sequence up-up-down-down[16] (u2d2 phase); the HFP is expected to be pseudoferromagnetic with a canted antiferromagnetic structure.[1,2] In the remainder of the paper we use the notation that the LFP-PP transition occurs at T_N. We also associate the HFP-PP transition with T_c, and the LFP-HFP transition with T_{lh}.

A. Zero-field specific-heat results

1. General comments

The dominant feature of the $H=0$ data shown in Figs. 4 and 5 is the extremely sharp peak, which corresponds to the specific heat changing by nearly 2 orders of magnitude for a change in temperature of only 100 μK. This is the clear signature of a first-order transition. The peak is not infinitely sharp because of small density gradients (Sec. III A 5) in the samples contained within the pores of the silver sponge (Sec. II A); different

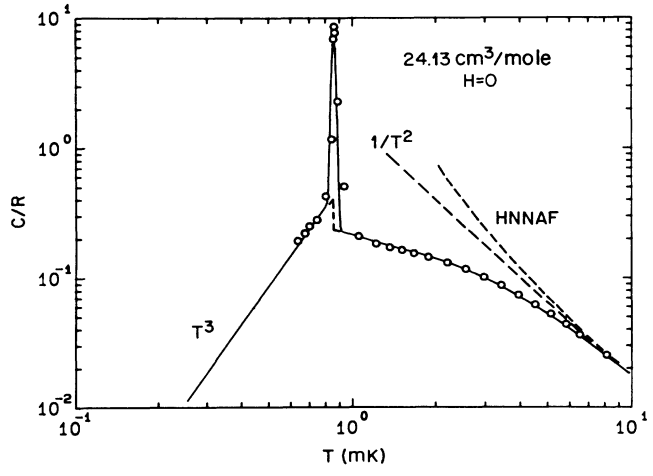

FIG. 4. ^{3}He specific heat at a molar volume of 24.13 cm^3 and in zero magnetic field. Also shown is the specific heat of a Heisenberg nearest-neighbor antiferromagnet computed using the ten-term high-temperature series expression from Ref. 21.

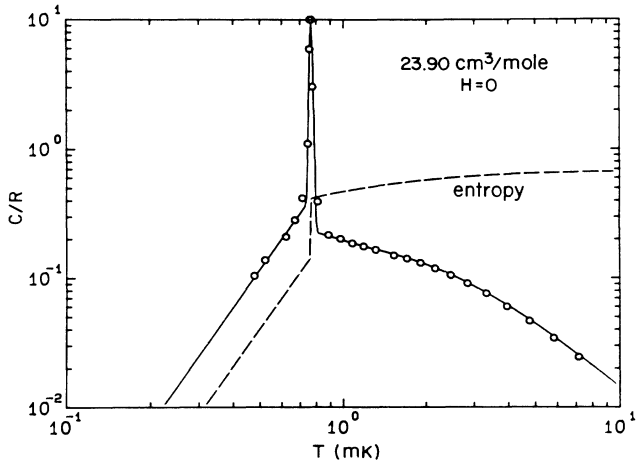

FIG. 5. ^{3}He specific heat at a molar volume of 23.90 cm^3 and in zero field.

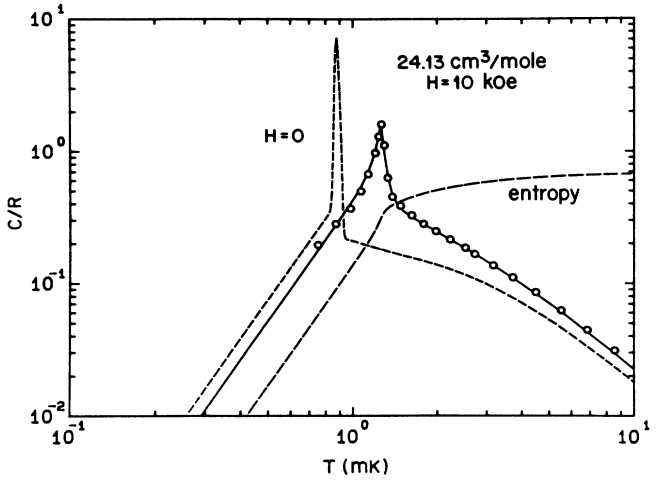

FIG. 6. ^{3}He specific heat at a molar volume of 24.13 cm^3 and in a magnetic field of 10 kOe. The long-dashed curve shows the implied entropy. Also shown for comparison are the smoothed specific-heat results obtained in zero field.

portions of the sample pass through the transition at slightly different temperatures. The sample at 23.90 cm^3/mole was grown more slowly than the lower-density sample and exhibits a somewhat sharper peak. The short-dashed curves near T_N in Fig. 4 show the expected behavior of the specific heat neglecting the contribution from the latent heat.

For temperatures below T_N the data at both densities are consistent with $C \propto T^3$. This is the expected T dependence because the elementary excitations are the spin waves, which, for an antiferromagnetic structure, have a linear dispersion relation.

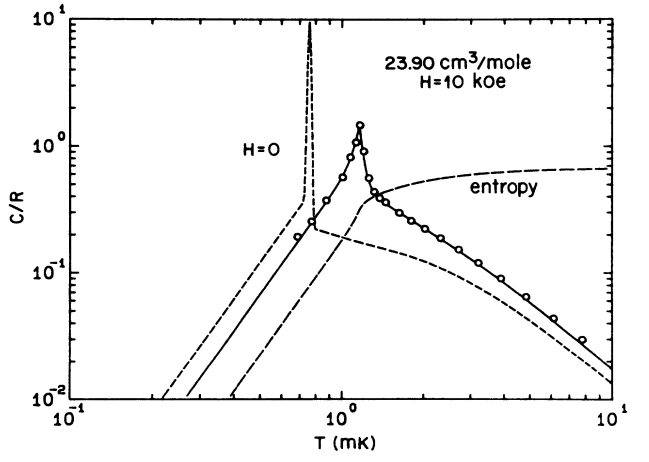

FIG. 7. ^{3}He specific heat at a molar volume of 23.90 cm^3 and in a magnetic field of 10 kOe. The long-dashed curve shows the implied entropy. Also shown for comparison are the smoothed specific-heat results obtained in zero field.

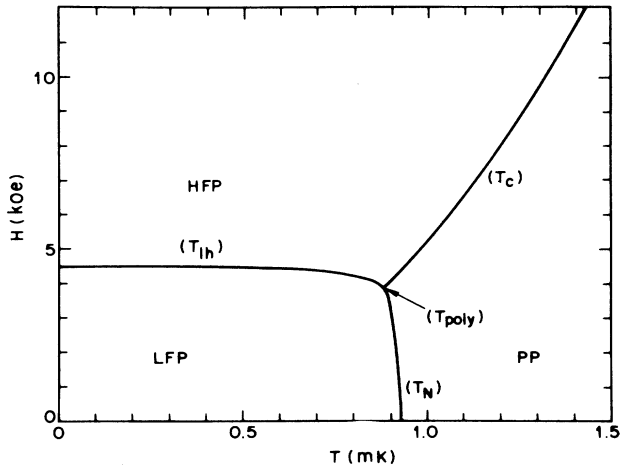

FIG. 8. Field-temperature phase diagram for bcc ^{3}He at melting density showing the notation use in the text.

For $T \gg T_N$ the data are tending towards a $1/T^2$ temperature dependence. This is the high-T temperature dependence for the specific heat of a two-level system. The splitting in the ground state is due to the exchange interactions between the ^{3}He nuclear spins.

Assuming that the ^{3}He nuclear-spin system can be described by a Heisenberg Hamiltonian, the high-T series expansion[17–19] for the $H=0$ specific heat is

$$C(T,0)/R = 3\beta^2 J_{xx}^2 - 3\beta^3 J_{xxx}^3 + \cdots , \quad (2)$$

where J_{xx}, etc. are particular moments of the unspecified exchange Hamiltonian and $\beta = 1/k_B T$. The dashed straight line in Fig. 4, indicating the limiting high-T behavior, corresponds to the value of J_{xx} extracted from specific-heat measurements[20] performed above 50 mK. Also shown for comparison in Fig. 4 is the specific heat computed using the ten-term series expansion[21] of the Heisenberg nearest-neighbor antiferromagnet. The divergence of the calculated curve away from the experimental results is not unexpected since it has been known for a decade[22] that this simple model is inadequate for describing solid ^{3}He at low temperatures. Theoretical explanation[23] of the experimental results for the specific heat requires the inclusion of more complicated exchange processes.

2. *Comparison with previous specific-heat results*

There have been only two other experiments performed which directly measure the specific heat of solid ^{3}He near the ordering transition: the early measurements of Dundon and Goodkind[24] and the very recent work by Sawada *et al.*[25] These two sets of data, each with a precision of roughly 10% or 20%, are represented by dashed curves in Fig. 9, where a comparison is made with the present work. In all three experiments the standard heat-pulse technique was used to measure the specific heat of solid ^{3}He samples contained within

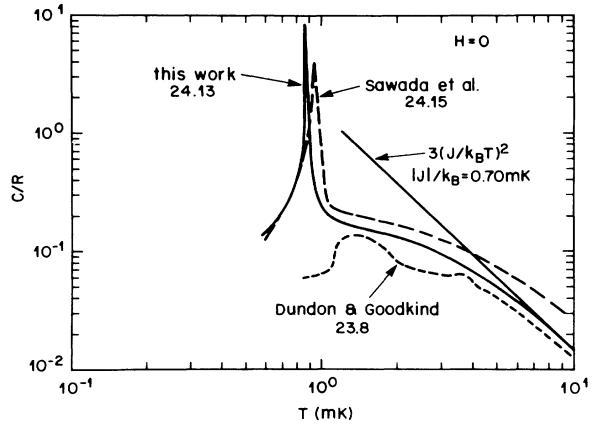

FIG. 9. Comparison with previous direct measurements of the specific heat of low-density solid ^{3}He.

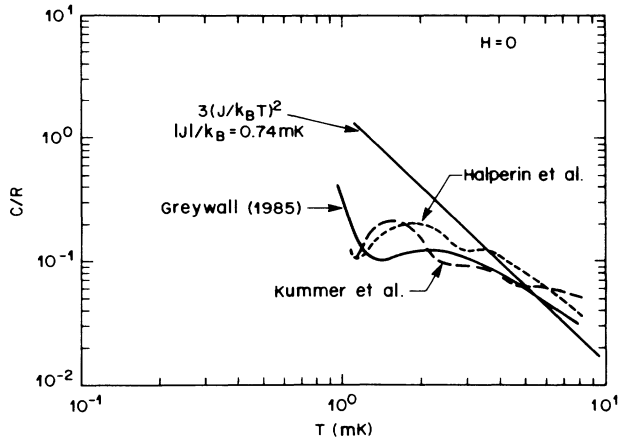

FIG. 10. Specific heat extracted from pressure-temperature measurements for ^{3}He on the melting curve.

the small pores of copper or silver powder sponges. In addition to the much smaller specific-heat values near 1 mK, the Dundon-Goodkind data also exhibit two bumps for temperatures greater than T_N. There is no evidence for either of these features in the more recent experiments.

Although the results of Sawada *et al.* are qualitatively quite similar to ours, there are significant quantitative differences. The broader and less symmetric peak at T_N may simply be due to larger density gradients in their samples. More difficult to explain, however, is the large discrepancy near 10 mK. We note that the present data tend with increasing temperature towards the extrapolation of results[20] obtained above 50 mK where thermometry is much less of an issue.

The specific heat of solid ^{3}He along the melting curve can also be inferred from measurements of the melting pressure versus temperature using the thermodynamic relation $C_m(T)=T(dS/dT)_m$ and the Clausius-Clapeyron equation

$$S_{s,m}(T)=S_{l,m}(T)-(V_{l,m}-V_{s,m})\left[\frac{dP}{dT}\right]_m . \tag{3}$$

In the low mK range the main contribution to the specific heat is determined by the term in d^2P/dT^2; consequently, the melting pressure must be measured extremely accurately. The results are also sensitive to the choice of the empirical expression used to fit the P-versus-T data.

The solid curve in Fig. 10 was computed using the P-T relation and liquid-helium specific-heat results from Ref. 12. The difference between the liquid and solid molar volumes was taken to be constant and equal to 1.314 cm^3/mole.[3] Except for the shallow minimum near 1.5 mK, this specific-heat curve is very similar to the present (but higher-density) results shown in Figs. 4 and 5. The shallow minimum in the specific heat computed for the melting curve presumably reflects the inadequacy of the fitting function used to describe the P-T data, for temperatures near T_N.

Also shown in Fig. 10 are the specific-heat curves based on the melting curves measured by Halperin *et al.*[3] and by Kummar *et al.*[4] In these experiments the temperature scale was based on measurements of the ^{3}He latent heat of solidification. Both of these curves show a complicated structure with peaks appearing above T_N, in qualitative agreement with the Dundon-Goodkind curve shown in Fig. 9. Halperin *et al.* have ruled out their peak near 2 mK being an artifact of their data analysis. Nonetheless, it seems probable[12] that the unexpected peaks above T_N are due to errors in the respective temperature scales.

The issue of the possible existence of a second specific-heat peak at $H=0$ is important since recent mean-field calculations by Stipdonk and Hetherington[26] and also numerical calculations by Cross and Bhatt[27] have suggested this possibility. Again, our data show no evidence of any anomalous structure.

3. *Spin-wave velocities and transition temperatures*

The molar specific heat and the average spin-wave velocity are related by

$$\frac{C}{R}=\frac{2n}{15}\frac{\pi^2 V}{N}\left[\frac{k_B T}{\hbar v_{\rm spin}}\right]^3 , \tag{4}$$

which is analogous to the expression for phonons. In the LFP, n (the number of modes) is two. Equation (4) is strictly valid for $T \ll T_N$; however, via their melting-pressure measurements, Osheroff and Yu[28] have demonstrated that the specific heat retains a T^3 temperature dependence to very near T_N. This is also consistent with our findings. With T measured in mK, V in cm^3/mole, and $v_{\rm spin}$ in cm/sec, Eq. (4) can be written as

$$v_{\rm spin}=\left[\frac{4.90nV}{C/RT^3}\right]^{1/3} \tag{5}$$

Values of T_N and $v_{\rm spin}^{\rm LFP}$ extracted from our specific-heat measurements are listed in Table I and are plotted versus the molar volume on log-log scales in Fig. 11. For comparison, the solid straight line shows $|J_{xx}|/k_B$ from Ref. 20. In that work it was determined, in good agreement with other experiments, that

$$|J_{xx}|/k_B = 3.04\times 10^{-24} V^{16.9} , \tag{6}$$

with $|J_{xx}|/k_B$ in mK.

The $H=0$ results for both T_N and $v_{\rm spin}^{\rm LFP}$ are, within experimental uncertainties, consistent with the same molar-volume dependence. This would be the expected result if there were a dominant exchange process. But various experimental findings, including the present specific-heat results above T_N, indicate that there must be several competing interactions. The unsetting conclusion seems to be that all of these exchange processes must have a very similar molar-volume dependence. The observation that $T_N \propto |J_{xx}|$ was first made by Hata *et al.*[29]

The values of T_N (Ref. 12) and $v_{\rm spin}^{\rm LFP}$ (Ref. 28) plotted in Fig. 11 at a molar volume of 24.22 cm^3 correspond to measurements performed on the melting curve with bulk samples of solid helium. The general agreement between these quantities and the respective values obtained for the samples contained within the pores of silver sinter is evidence that there are no serious size-effect problems. We note too that the spin-wave velocity plotted in Fig. 11 and attributed to Osheroff and Yu,[28] namely 7.7 cm/s, is smaller than the value they actually reported, 8.4±0.4 cm/s. The difference corresponds to our using their melting-pressure data obtained above 0.4 mK rather than at lower temperatures and also to the correction needed because of the different T scales used.

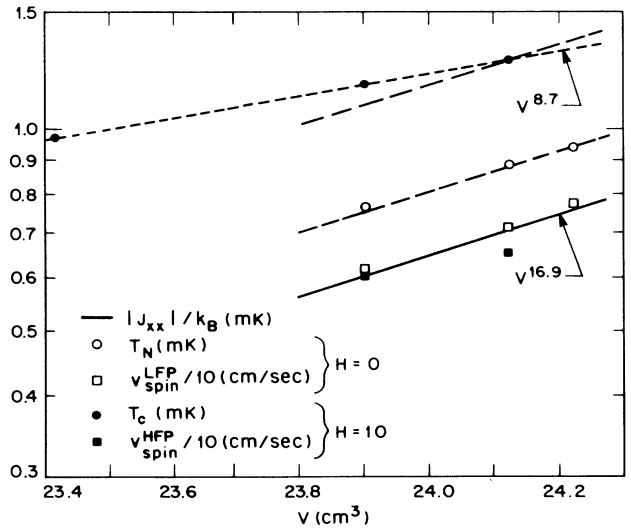

FIG. 11. The molar volume dependence of T_N and $v_{\rm spin}^{\rm LFP}$ at $H=0$ compared with that for T_c and $v_{\rm spin}^{\rm HFP}$ at $H=10$ kOe. The solid curve for $|J_{xx}|$ is based on data from Ref. 20.

4. *Empirical expressions for C at H = 0*

If, as suggested by the T_N and $v_{\rm spin}^{\rm LFP}$ results, all relevant energies have an identical density dependence, then the two sets of specific-heat results showns in Figs. 4 and 5 should be related, over the complete temperature range, by a simple rescaling of the temperature. That is, the data when plotted on log scales should differ only by a uniform displacement along the T axis. To within the precision of the measurements, we find this to be true. Consequently, we write the zero-field specific heat as a universal function of $T/T_N(V,0)$.

Below $T_N(V,0)$

$$C/R = 0.43(T/T_N)^3 . \tag{7}$$

For temperatures between 1 and 8 mK, a least-squares fit yielded

$$C/R = \sum_{n=2}^{7} a_n (T_N/T)^n , \tag{8}$$

with

$$a_2 = 3.0683, \quad a_3 = -9.817 ,$$
$$a_4 = 13.6917, \quad a_5 = -8.8361 ,$$
$$a_6 = 2.0135, \quad a_7 = 0.1097 .$$

The rms deviation from the fit is 0.5%. The data very near T_N which were obviously affected by the latent-heat contribution (see Sec. III A 5) were excluded from this analysis. In addition to describing the experimental results above $1.2T_N$, Eq. (8) also provides a reasonable extrapolation of the high-T results down to about $0.8T_N$. It should be stressed that Eq. (8) is only an empirical description of the data. Because of the large number of parameters and the strong correlations between these parameters, no significance should be placed on any of the individual values.

Smoothed results for C/R and S/R based on Eqs. (7) and (8) are shown in Fig. 12 plotted on linear scales. The specific-heat curve neglects the latent heat. Our determination for the jump in entropy at T_N is

$$\Delta S/R \ln 2 = 0.41\pm 0.02 . \tag{9}$$

This value is comparable to previous determinations;[25,28,30] however, there is a quantitative discrepancy with the most precise of these earlier results. From measurements of the melting pressure near T_N, Osheroff and Yu determined, via the Clausius-Clapeyron equation, $S^-/R \ln 2 = 0.19$ and $S^+/R \ln 2 = 0.68$. These values have been adjusted to our temperature scale. Our corresponding values are 0.21 and 0.61. The uncertainty in all four of these numbers is roughly 0.01. The difficulty is thus localized to the results for S^+. We note though that our melting-curve slope from Ref. 12 implies $S^+/R \ln 2 = 0.62$, in good agreement with our present determination.

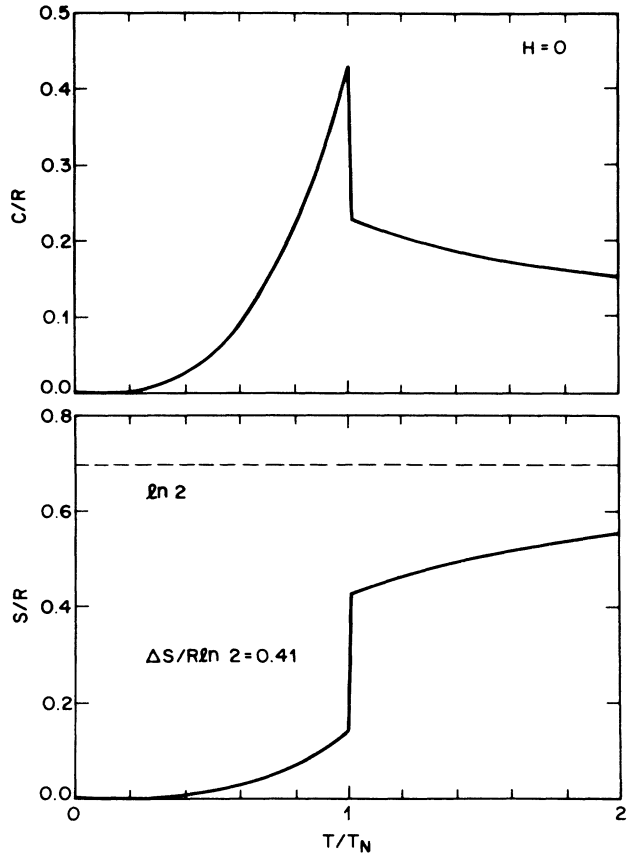

FIG. 12. Smoothed results for the specific heat and entropy of low-density solid ^{3}He determined using Eqs. (7) and (8).

5. *Density gradients*

The density gradients in our solid ^{3}He samples (grown via the blocked-capillary technique) can be inferred from the zero-field specific-heat data, knowing that this transition is first order. This information will be used later (Sec. III B 1) in support of our claim that the HFP-PP transition is second order.

We assume first that the true specific heat of a uniform-density sample can be described well for temperatures near T_N by the short-dashed curves in Fig. 4 which are just simple extrapolations of the behavior observed away from the transition. We also assume that the local molar volume follows a Gaussian distribution with the fraction of the sample within dV of V being given by

$$f(V)dV=(\gamma/\sqrt{\pi})e^{-\gamma^2(V-V_0)^2}dV \ . \tag{10}$$

The latent heat due to the fraction of the sample with transition temperatures between T_N and T_N+dT_N is therefore

$$dQ_{\text{latent}}=f(V)\frac{dV}{dT_N}dT_N nL(V) \ , \tag{11}$$

where L is the molar latent heat and n is the total number of moles of sample. As discussed in the preceding subsection, the size of the jump in entropy at T_N is found to be independent of molar volume and equal to $0.41R$ ln2. Therefore,

$$L(V)=T_N(V)\Delta S=0.41T_N R \ln 2 \ . \tag{12}$$

The derivative of Eq. (11) can be evaluated using the molar-volume dependence of T_N given by Eq. (6), namely $T_N \propto V^{16.9}$.

For temperatures near T_N, energy applied to the sample goes both towards supplying the necessary latent heat and also towards raising the temperature, i.e.,

$$dQ=nC\,dT+dQ_{\text{latent}} \ . \tag{13}$$

Therefore,

$$\frac{C_{\text{meas}}}{R}\equiv\frac{1}{nR}\frac{dQ}{dT}=\frac{C}{R}+\frac{1}{nR}\frac{dQ_{\text{latent}}}{dT_N} \ . \tag{14}$$

Here, C is the molar specific heat that would be measured in the absence of any latent heat and is given approximately by the ideal behavior indicated again by the short-dashed stepped curve in Fig. 4. Combining Eqs. (11), (12), and (14),

$$\frac{C_{\text{meas}}(T)}{R}=\frac{C_{\text{ideal}}(T)}{R}+0.0168Vf(V) \ . \tag{15}$$

V is the molar volume corresponding to a transition at temperature T. The smooth curves in Figs. 4 and 5 which fit the data in the vicinity of the peak very well correspond to γ values [Eq. (10)] of 30 and 40 cm^{-1}, respectively. $\gamma=40$ implies that 90% of the sample had a local molar volume within 0.03 cm^3 of the average value.

B. Specific-heat results for $H>0$

1. *Order of the HFP-PP transition*

The specific-heat data obtained in a field of 10 kOe, Figs. 6 and 7, exhibit peaks which appear to be qualitatively quite different from the zero-field results, indicated for comparison by the dashed curves. An immediate conclusion, which we support later, is that if the zero-field transition is first order the transition at 10 kOe (and also at 6 kOe) cannot be. This statement could be reconciled with the claim by others[31,32] that the HFP-PP transition is first order, at least at somewhat smaller fields, if there were a tricritical point on the T_c line in the vicinity of 5 kOe. However, there are other very recent (nonequilibrium) measurements[30] which suggest that there is no latent heat liberated at T_c in the field range between 4 and 5 kOe. The proposal that the "transition" might be only the Schottky ordering of the ^{3}He spins by the external field is ruled out by the sharpness of the measured specific-heat peaks.

The specific-heat results at 6 and 10 kOe and at two molar volumes are plotted on linear scales in Fig. 13. The three sets of data plotted in this manner nearly coincide, with the composite set of data exhibiting a peak which is suggestive of a λ-type transition.

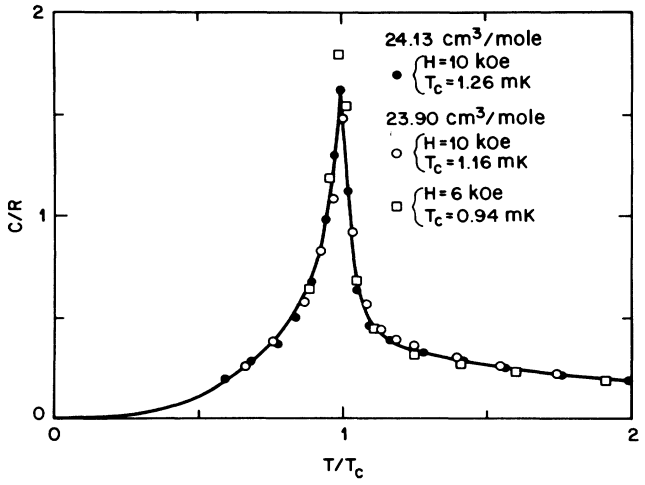

FIG. 13. Reduced plot of the specific heat measured near T_c at two different molar volumes and at two magnetic fields. The composite set of data exhibits a peak characteristic of a λ-type transition.

As explicitly demonstrated in Fig. 14, the width and shape of this peak are inconsistent with this transition being first order. The solid curve shows the smooth experimental results. The dashed curve shows the expected specific heat, if the transition were first order. This curve was computed using the sample density distribution inferred from the $H=0$ results (Sec. III A 5) and an estimate of the "latent heat" based on the measured specific heat away from T_c.

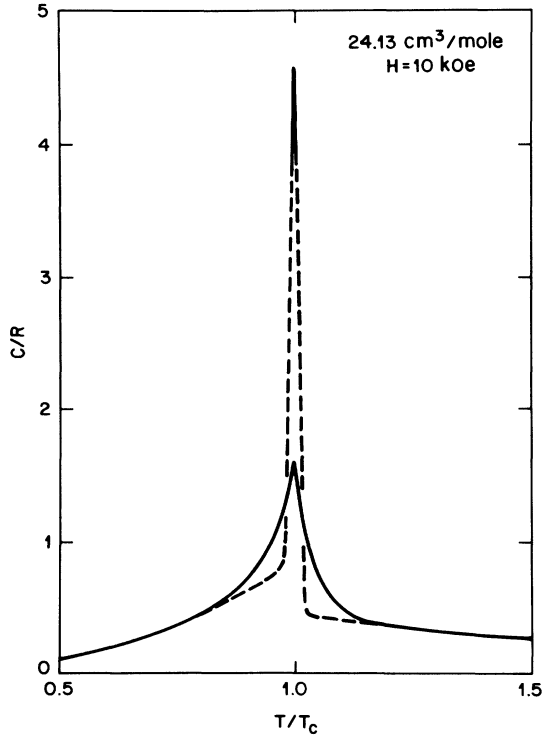

FIG. 14. Comparison of the measured specific heat near T_c with that expected if this transition were first order.

Although it is not possible to completely rule out a small latent heat at T_c at lower fields, we proceed with the assumption that the HFP-PP transition is a continuous second-order transition from at least 10 kOe down to the polycritical point. This conclusion is based on the melting-pressure measurements of Tang *et al.*,[30] the magnetization measurements of Prewitt and Goodkind[33] (to be discussed in Sec. III C), and on our own specific-heat data.

2. *Molar volume dependence of T_c and v_{spin}^{HFP}*

The T_c values measured in a field of 10 kOe are shown plotted versus the molar volume in Fig. 11, where comparison is made to T_N at $H=0$. This transition temperature shows a much weaker density dependence than $T_N(0)$, as we verified with an additional determination of T_c at 23.418 cm^3/mole. Assuming a simple power-law dependence leads to $T_c(10)\propto V^{8.7}$. Although this exponent is only slightly more than half of the corresponding exponent for $T_N(0)$, it is nevertheless also consistent with all exchange energies being proportional to V^{17}. This consistency is demonstrated in Fig. 15, where the T_c values measured at 10 kOe are shown on a reduced plot of H versus T_c. If all of the exchange energies are shifted by a uniform factor f when the density is changed, then the thermodynamic properties of the system can be expressed as a universal function of H/f and T/f. The scaling of the axes in Fig. 15 is under the further assumption that the energies scale as V^x. The reference volume is taken to be that corresponding to the sample at melting pressure. Our expectation is that the results plotted for a particular value of x, namely 17, should coincide with the melting-pressure T_c-versus-H curve, and we find this to be true within our uncertainties. Unfortunately, considerably more weight must be given to the points at the two larger molar volumes, since the solid curve [based on Eq. (39)] is only an extrapolation of T_c results obtained below 10 kOe.

Although the HFP specific-heat data obtained below T_c do not extend to low enough temperatures to allow an accurate determination of the temperature dependence, they are consistent with a T^3 temperature dependence. The T^3 behavior is expected on the basis of previous melting-pressure experiments, which extend to much lower temperature, and also as a consequence of our claim that the HFP-PP transition is second order. The spin-wave velocities extracted from the ordered-phase data, assuming a single spin-wave mode, are also plotted in Fig. 11. Although less precise than the T_c determinations, the results for $v_{\rm spin}^{\rm HFP}$ show a very similar volume dependence. This leads us [see Eq. (4)] to describe the low-density, low-temperature HFP data at 10 kOe by the relation

$$\frac{C}{R}(V,10)=0.86\left[\frac{T}{T_c(V,10)}\right]^3 . \tag{16}$$

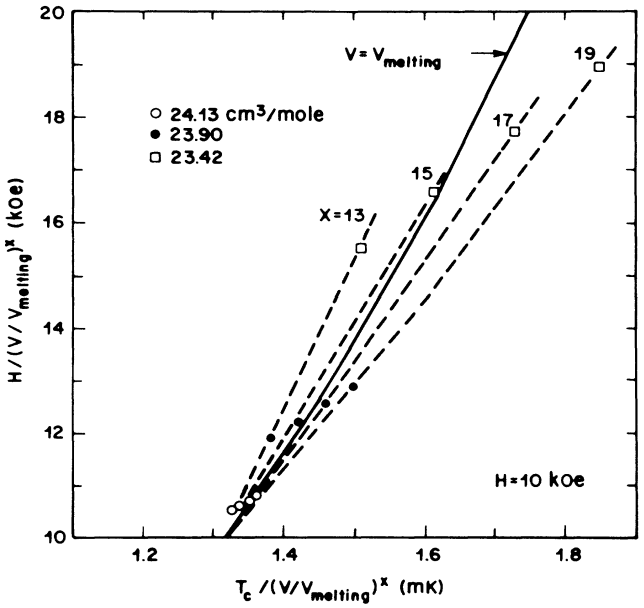

FIG. 15. Reduced plot of H vs T_c showing T_c values obtained at 10 kOe and at three different molar volumes. The points nearly coincide with the extrapolated curve for $T_c(H)$ at melting density if $x \approx 17$.

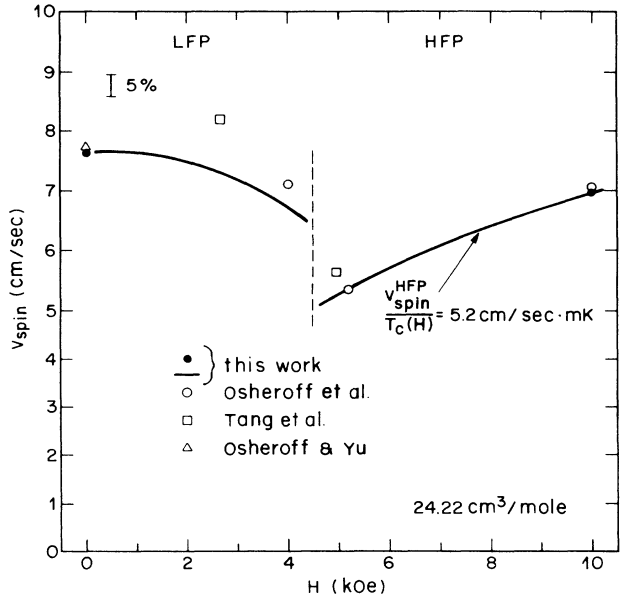

FIG. 16. Field dependence of the spin-wave velocity at melting density. Comparison is made with previous results in both the low-field phase and high-field phase.

This equation is obviously consistent with the universal behavior of the low-temperature specific heat when plotted as a function of T/T_c, Fig. 13. The fact that the 6 kOe results also fall on this same curve in Fig. 13 suggests the generalization

$$\frac{C}{R}(V,H)=0.86\left[\frac{T}{T_c(V,H)}\right]^3 . \tag{17}$$

Further support for this relation is given in the following subsection.

3. *Field dependence of v_{spin}^{LFP} and v_{spin}^{HFP}*

Figure 16 shows the spin-wave velocity plotted versus magnetic field at melting density, i.e., at 24.22 cm^3/mole. Our results at 0 and 10 kOe were extrapolated to this molar volume using Eqs. (7) and (17), respectively. All of the other data points plotted derive from melting-pressure measurements above 0.4 mK and have been adjusted to our temperature scale. This correction reduces these velocities by roughly 15%. At 0 and 10 kOe the agreement with Osheroff and Yu[28] and with Osheroff, Godfrin, and Ruel[34] is within a few percent.

The solid curve for the HFP is based on Eq. (17), which, together with Eq. (4), yields

$$v_{\rm spin}^{\rm hfp}=5.17T_c \tag{18}$$

for the velocity in cm/s and T_c in mK. $T_c(H)$ will be discussed in Sec. III D 2 and is given by Eq. (39). Near 5 kOe the curve agrees well with the plotted points, especially the value from Ref. 34.

The solid curve drawn for the LFP is based on

$$\frac{C}{R}=(0.43+0.003\,17H^3)[T/T_N(0)]^3 , \tag{19}$$

with H measured in kOe. The field dependence of C was inferred from a thermodynamic analysis of the phase diagram which will be discussed in Sec. IV D. A decreasing velocity with increasing field implies that the entropy, at fixed temperature, is increasing. This is the behavior expected for an antiferromagnet. For the HFP, which is pseudoferromagnetic, the opposite effect is observed. At the LFP-HFP boundary the LFP has the smaller entropy which must be true since H_{lh} decreases with increasing temperature. The difference between our results at 4 kOe and the measurement from Ref. 34 is 6%. This is within the combined uncertainties.

4. *C at "high" temperature, $H > 0$*

The generalized high-temperature series expression for the increase in the specific heat induced by a small applied magnetic field is

$$\frac{\Delta C}{R}=\frac{C(T,V,H)}{R}-\frac{C(T,V,0)}{R}$$
$$=\left[\frac{\mu H}{k_B T}\right]^2\left[1+12\frac{J_{xzz}}{k_B T}+72\left[\frac{J_{xxzz}}{k_B T}\right]^2+\cdots\right] . \tag{20}$$

Obviously, if the temperature is not large compared to $|J|/k_B$, many terms must be retained in the series. Consequently, for the range of temperatures covered in

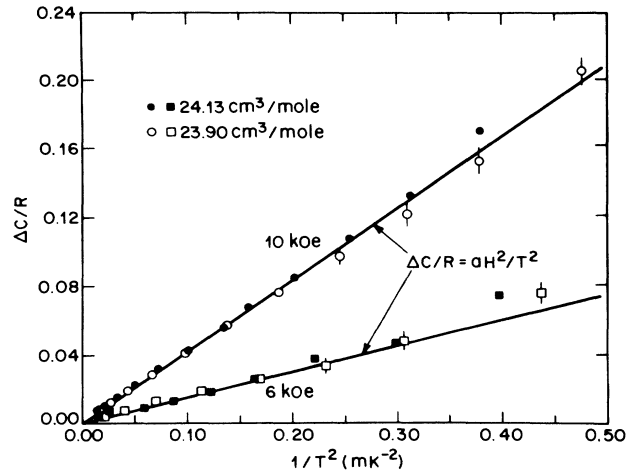

FIG. 17. Increase in the specific heat induced by an applied magnetic field. Results are shown for fields of 6 and 10 kOe and for two different densities.

the present experiment we would expect ΔC to have a rather complicated temperature dependence. The experimental results show, however, that this is not the case.

In Fig. 17, ΔC is plotted versus $1/T^2$ for fields of 6 and 10 kOe at two molar volumes. To within the precision of the measurements ($\sim 2\%$) and independent of the sample density, the results are described by

$$\frac{\Delta C(T,H)}{R} = aH^2T^2 , \tag{21}$$

with $a = 0.0042$ mK kOe^{-2}. This equation can also be rewritten as

$$\frac{\Delta C}{R} = \left[\frac{\mu_{\text{eff}}H}{k_B T}\right]^2 , \tag{22}$$

with $\mu_{\text{eff}} = 0.83\mu$ ($\mu/k_B = 0.078$ mK/kOe). That is, the free-spin relation can be used to describe the field-induced increase in the PP specific heat at low temperatures, if μ is replaced by an effective magnetic moment. This simple, but intriguing, relation suggests that it may be worthwhile to consider models different from the usual multiple-spin-exchange theories to describe solid ^{3}He at very low temperatures.

5. *Empirical expressions for C near T_c*

Empirical expressions are now given for the specific heat very near the T_c line, in order to complete the description of the low-density specific heat of solid ^{3}He for $T \lesssim 10$ mK and for $H \lesssim 10$ kOe. The complete set of expressions will be used later to determine other thermodynamic quantities and also in an analysis of the T-H phase diagram.

For $T \ll T_c$ the HFP specific-heat results are described by Eq. (17), while for $T \gg T_c$ the PP results are described by Eqs. (8) and (21). Near T_c the measured specific heat is considerably larger than that computed using these equations. The difference, which shows a step discontinuity at T_c, is defined as C_{ex}. The size of this step is given by

$$\frac{\delta C}{R} = \frac{C^{\text{HFP}}(T_c)}{R} - \frac{C^{\text{PP}}(T_c)}{R} . \tag{23}$$

We also define

$$\frac{\delta S}{R} \equiv \ln 2 - \int_{T_c}^{\infty} \frac{C^{\text{PP}}}{RT} dT - \int_0^{T_c} \frac{C^{\text{HFP}}}{RT} dT . \tag{24}$$

The excess specific heat below T_c is described well by

$$\frac{C_{\text{ex}}}{R} = \alpha (T/T_c)^{20} . \tag{25}$$

For $T > T_c$,

$$\frac{C_{\text{ex}}}{R} = \left[\alpha + \frac{\delta C}{R}\right](T/T_c)^{-28} . \tag{26}$$

Thermodynamic consistency requires

$$\frac{S_{\text{ex}}}{R} = \frac{\alpha}{20} + \frac{\alpha + \delta C/R}{28} = \frac{\delta S}{R} , \tag{27}$$

which becomes the defining equation for the parameter $\alpha(V,H)$.

The smoothed curves passing through the data points in Figs. 4–7 and also in Figs. 13 and 14 were computed using the empirical equations for the specific heat.

Figure 18 shows the entropy at melting density obtained by integrating the smoothed results for C/T. The number associated with each of the curves gives the field in kOe. The dashed curve shows T_c for the curves with $H \geq 4$ kOe. At T_c, $S/R \ln 2 \lesssim 0.5$.

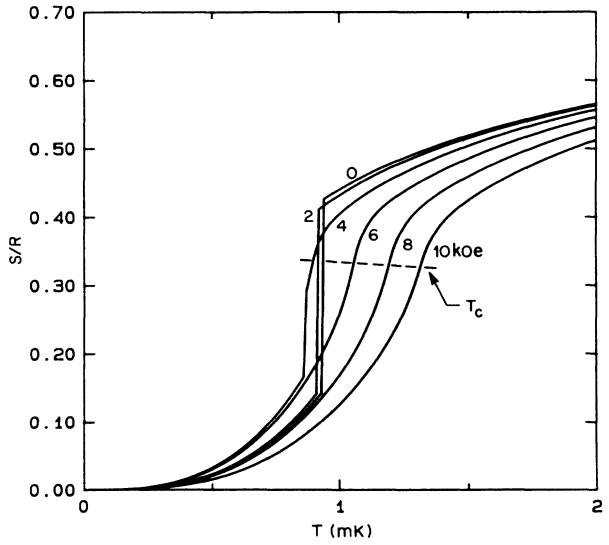

FIG. 18. Smoothed results for the entropy derived from specific-heat measurements. The curves are plotted for several magnetic fields between 0 and 10 kOe.

C. Magnetization

A check for consistency with other thermodynamic data, obtained from very different types of measurements, can be made by applying the Maxwell relation

$$\left[\frac{\partial M}{\partial T}\right]_H = \left[\frac{\partial S}{\partial H}\right]_T \tag{28}$$

to the empirical equations for the entropy and extracting values for the magnetization. The assumption, of course, is that the simple empirical equations are sufficiently accurate to justify this type of analysis.

Equations (21) and (22) for the specific heat in the paramagnetic phase implies quite directly

$$M(T)=aRH/T \tag{29}$$

or, equivalently, the Curie relation

$$\chi=aR/T=R\left[\frac{\mu_{\rm eff}}{k_B}\right]^2\frac{1}{T}\ . \tag{30}$$

These equations are expected to be valid for $T<5$ mK. At higher temperatures the relative uncertainty on the field-induced contribution to the specific heat becomes very large, and it is this term which leads to Eqs. (29) and (30). One immediate test of our results can be made by comparing our susceptibility at T_A (the superfluid transition temperature of liquid ^{3}He at melting pressure) with previous determinations. Our value for $10^4\chi$ is 1.40 ± 0.05 mole^{-1}. Osheroff and Anderson,[35] Kummer *et al.*,[4] and Godfrin[36] find respective values of 1.44, 1.53, and 1.49 with uncertainties of about 0.03. We note that all three of these values derive, via a Clausius-Clapeyron relation, from measurements of the field dependence of the melting pressure at T_A and are independent of temperature scale.

Our results can also be compared with the direct magnetization measurements of Prewitt and Goodkind.[33] These authors made measurements in the temperature range 0.5–2 mK using a superconducting quantum-interference device (SQUID) magnetometer and also found M/H to be independent of H at sufficiently high temperatures. Their universal curve is consistent with a $1/T$ temperature dependence and with a coefficient within 10% of the new value.

The high-temperature series expression for the molar susceptibility is

$$\chi=R\left[\frac{\mu}{k_B}\right]^2\frac{1}{T}(1+4\beta J_{xzz}+12\beta^2J_{xxzz}^2+\cdots)\ . \tag{31}$$

For temperatures not too low this relation can be rewritten as

$$\chi=\frac{R(\mu/k_B)^2}{T-\Theta}\ , \tag{32}$$

where $\Theta=4J_{xzz}$. This Curie-Weiss relation with $\Theta\approx-2$ mK describes experimental data well for $T\gtrsim10$ mK.

In Fig. 19, $HM_{\rm sat}/M$ is plotted versus T. Here, $M_{\rm sat}$ is the saturation magnetization, $N\mu=6.472$ Oe/mole.

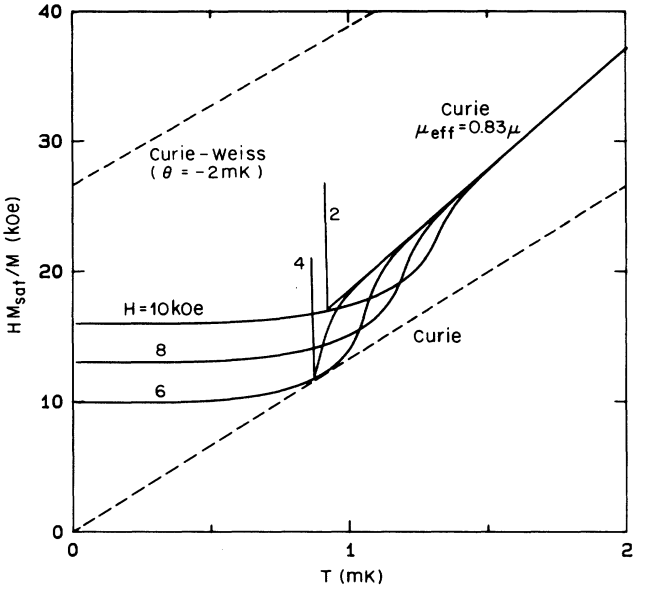

FIG. 19. Smoothed results for H/M computed using Eqs. (33) and (34) at several different magnetic fields. Comparison is made with both the Curie and Curie-Weiss relations.

The dashed curves, to be compared with our higher-temperature results, correspond to the Curie and Curie-Weiss relations. The departure from the Curie-Weiss curve observed at low temperatures can be explained as being due to the higher-order terms in Eq. (31), but it is also possible to interpret the experimental results as exhibiting a rather sharp crossover from Curie-Weiss behavior to Curie behavior with an effective moment only 20% smaller than the true moment.

For $T\approx T_c$, there is an additional contribution to the paramagnetic magnetization corresponding to the excess specific heat given by Eq. (26). The complete empirical expression describing M for $T\gtrsim T_c$ is

$$M(T,H)=\frac{aRH}{T}+\frac{R}{27}\left[\frac{T}{T_c}\right]^{-27}\left[\alpha+\frac{\Delta C}{R}\right]\frac{dT_c}{dH}\ . \tag{33}$$

The second term implies a rapid rise in M as T_c is approached from higher temperatures. For $H\lesssim H_{\rm poly}$, the proximity of the second-order transition is treated by simply extrapolating the transition line into the LFP.

In the HFP, the expressions for the specific heat [Eqs. (17) and (25)] lead to

$$M(T,H)-M(0,H)=-R\left[\frac{dT_c}{dH}\right]\left[0.215\left[\frac{T}{T_c}\right]^4+\frac{\alpha}{21}\left[\frac{T}{T_c}\right]^{21}\right]\ . \tag{34}$$

With increasing temperature, the magnetization decreases away from its limiting zero-temperature value as

T^4 at low temperatures and much more rapidly near T_c. At extremely low temperatures the specific heat may deviate from a T^3 temperature dependence; consequently, the T^4 dependence for M may also be incorrect in the limit $T \to 0$.

Values for $M(0,H)$ in the HFP are determined by evaluating Eqs. (33) and (34) at T_c. The results are shown in Fig. 20 plotted as a solid curve. $M/M_{\rm sat} \approx 0.60$ agrees reasonably well with other more direct determinations,[33,34,37,38] especially the very recent and precise values of Osheroff *et al.*,[34] which are shown plotted as open circles in the figure. A quantitative comparison with their values, however, is meaningful only at the higher fields. At the lower fields our curve is not independent of their results since our T_c-versus-H transition line [i.e., dT_c/dH in Eqs. (33) and (34)] was determined in part using their magnetization results. This will be discussed in Sec. III D.

Smooth curves for $HM_{\rm sat}/M$ versus T determined using Eqs. (33) and (34) are shown in Fig. 19 at several constant fields. These curves can be compared with the results of Prewitt and Goodkind,[33] who have plotted their data obtained for fields between 0.8 and 5.8 kOe in a similar manner. Their curves are qualitatively similar and also show, with decreasing temperature, the smooth breaking away from the limiting high-temperature behavior. This is indicative of a second-order transition. We note that Prewitt and Goodkind took the onset of these departures, rather than the inflection point of the curves, as the indicator for T_c, which explain their T_c's being roughly 0.1 mK too high. Their results are consistent with our assumption that the HFP-PP transition remains second order between 6 kOe and the polycritical point.

For the LFP, Eq. (19) for the specific heat leads to

$$M(T,H)-M(0,H)=0.000\,65RT^4H^2/T_N(0)^3\ , \quad (35)$$

which implies that the magnetization increases relative to its zero-temperature value with increasing temperature. That is, the effect of increasing temperature is to decrease the amount of antiferromagnetic order. In evaluating Eq. (35), we have taken $M(0,H)$ from Osheroff *et al.*,[34] who find $M^{\rm LFP}(0,H)/M_{\rm sat}H = 0.020$ kOe^{-1}.

Comparison is made to some previous results for M/H in small magnetic fields in Fig. 21. The temperatures have been normalized so that T_N coincides with our determination. The solid curve was computed using Eqs. (29) and (35) with $H = 0.8$ kOe, which corresponds to the field at which Prewitt and Goodkind obtained the data shown as open circles. The long-dashed curve was computed for $H = 0.26$ kOe for comparison with the data of Hata *et al.*[29] Their smooth results are represented by the short-dashed curve, which has been normalized to agree with our curve at 2 mK. These two sets of results agree reasonably well. We note, in particular, the small increase in their M/H values for $T \lesssim T_N$, which is predicted by our Eq. (19). The temperature dependence of M/H observed by Prewitt and Goodkind in the LFP, but at a larger field, is steeper than that of Hata *et al.* This is also consistent with our relation, as are the 4-kOe results from Ref. 33 (not shown in Fig. 20). These latter data show a temperature dependence near T_N which is about 4 times stronger than the 0.8-kOe results.

As a possible explanation for the fact that the Prewitt-Goodkind data lie systematically below our curve, we speculate that a portion of their sample, contained within the pores of a sinter, may have been in the liquid state. The melting curve for ^{3}He in the pores of a sinter is shifted relative to that for the bulk,[39] but their stated molar volume is very close to that for bulk ^{3}He at melting.

In Fig. 22 the magnetization is plotted directly as a function of the temperature for several constant fields. Of the curves plotted, the behavior at 4 kOe in the LFP is subject to the largest uncertainties and needs testing

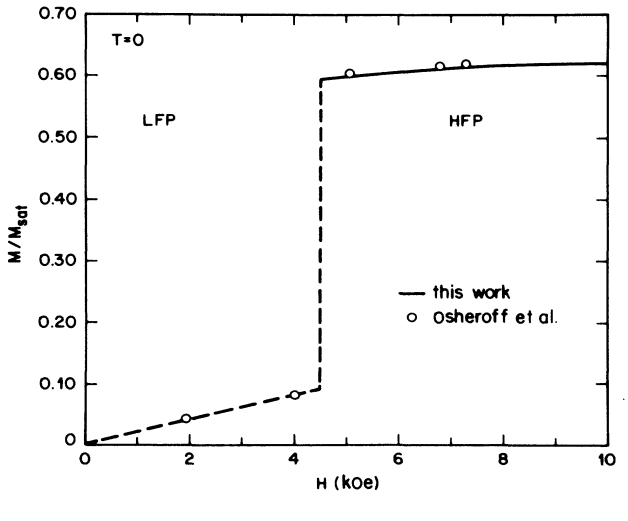

FIG. 20. Field dependence of the zero-temperature magnetization. The solid curve for the HFP is based on Eqs. (33) and (34). The data points plotted for both the LFP and HFP are from Ref. 34.

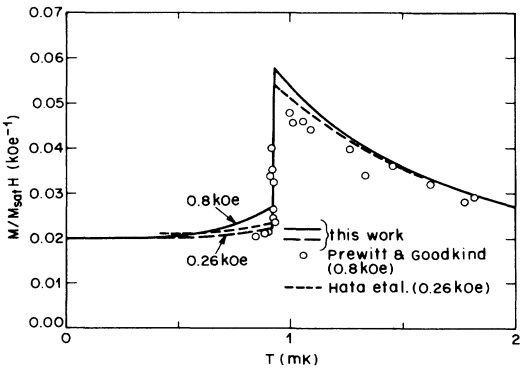

FIG. 21. M/H at small magnetic fields. Comparison is made with the work of Prewitt and Goodkind (Ref. 33) at 0.8 kOe and with the work of Hata *et al.* (Ref. 29) at 0.26 kOe.

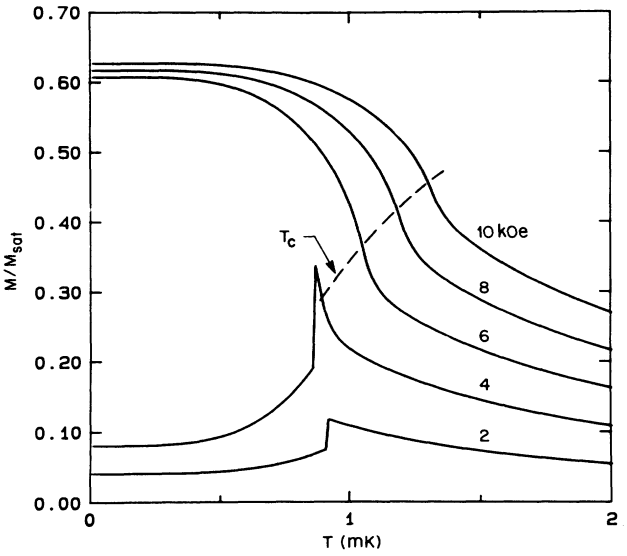

FIG. 22. Smoothed results for the magnetization of solid ^{3}He derived mainly from specific-heat measurements.

by direct measurements. We also note that unpublished NMR measurements by Osheroff and Ruel at 5.2 kOe show a much steeper change in M at T_c than that determined by our empirical expressions. This may suggest a much sharper transition close to the polycritical point than we see at higher fields.

D. Phase diagram

1. General comments

The field-temperature phase diagram for solid ^{3}He at melting pressure, Fig. 23, was first mapped out by Kummer *et al.*[4] more than ten years ago and has remained qualitatively unchanged by subsequent more precise measurements.[25,30,31,33] In fact, there is still not a quantitative consensus for the exact placement of the various phase boundaries. More importantly, there also remain uncertainties about the nature of the various transitions, particularly the transition separating the high-field and paramagnetic phases. It is generally conceded, though, that T_N versus H is a first-order line, which is certainly consistent with our zero-field specific-heat data.

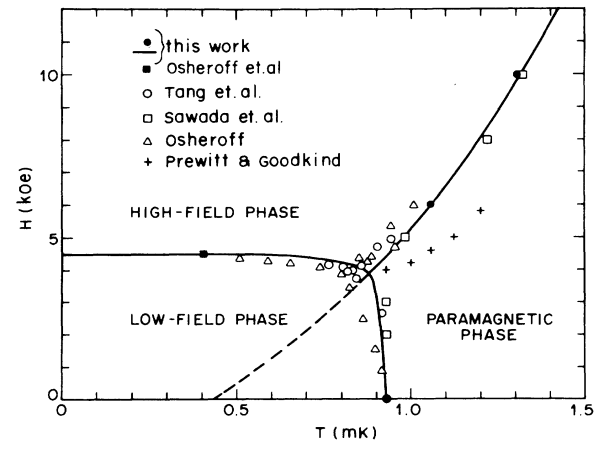

FIG. 23. Field-temperature phase diagram for solid ^{3}He at melting density. The solid curves are based on an analysis of thermodynamic data. The T_c-vs-H boundary is described by Eq. (39). Coordinates for the other boundaries are listed in Table II.

Our specific-heat results at fields of 6 and 10 kOe clearly show, at least for $H > 6$ kOe, that there is a second-order transition at T_c. At lower fields theoretical calculations suggest that there may be a tricritical point on the T_c line, below which the transition becomes first order. Although this issue has not yet been completely resolved experimentally, the existence of a tricritical point would seem to be inconsistent with the magnetization measurements of Prewitt and Goodkind[33] (see Sec. III C) and also with the very recent melting-pressure results of a Tang *et al.*[30] This latter group made measurements at several fields below 5 kOe and, to within the precision of their measurements, detected no latent heat at T_c. Moreover, their determinations of T_{lh} are a smooth continuation of their T_N values, i.e., there is no obvious discontinuity in the slope at $T_{\rm poly}$. This also implies, via the Clausius-Clapeyron equation, that there is no latent heat associated with the HFP-PP transition at $T_c = T_{\rm poly}$. As noted by Tang *et al.*, the H-T phase diagram for solid ^{3}He appears, therefore, to be similar to the P-T diagram for ^{4} He, where the λ line meets the melting curve.

The actual temperature and field coordinates of the polycritical point have been determined in many different experiments. All of these yield a value for $H_{\rm poly}$ of about 4 kOe. We adopt a value of 3.90 kOe. The uncertainty in $T_{\rm poly}$ is much larger, even if the various T scales used are normalized to agree at $T_N(0)$. It seems likely that in most cases this is attributable to the field-dependent boundary resistance between the solid ^{3}He sample and its container (see the Appendix). From the analysis discussed in the following subsection we determine $T_{\rm poly} = 0.88$ mK.

Two other special fixed points in the phase diagram are T_N at $H = 0$ and H_{lh} at $T = 0$. Based on the T scale of Ref. 12, $T_N(0) = 0.93$ mK. Osheroff *et al.*[34] find $H_{lh}(T = 0.4\ \text{mK}) = 4.492$ kOe. Note that the Clausius-Clapeyron equation

$$\frac{dH}{dT} = -\Delta S/\Delta M \tag{36}$$

requires the T_N line to be perpendicular to the temperature axis at $H = 0$, since $\Delta M \equiv M_{\rm PP} - M_{\rm LFP} \equiv 0$. It also requires that the T_{lh} line be perpendicular to the field axis at $T = 0$ since $\Delta S \equiv S_{\rm HFP} - S_{\rm LFP} \equiv 0$. Experimentally, it is found that, for small fields, $\Delta M \propto H$, while ΔS remains approximately constant. From this it follows (again from the Clausius-Clapeyron equation) that, in the limit $H \to 0$,

$$T_N(H) - T_N(0) \propto H^2 . \tag{37}$$

Assuming that the entropy in both the LFP and HFP retains its T^3 temperature dependence at very low temperatures, we have, for $T \to 0$,

$$H_{lh}(T) - H_{lh}(0) \propto T^4 . \tag{38}$$

2. T_c versus H; T_{poly}

In this subsection a relation between T_c and H at melting pressure is determined for fields between H_{poly} and 10 kOe. It is thermodynamically consistent and agrees well with our direct measurements of T_c at 6 and 10 kOe.

Shown in Fig. 24 as a dashed curve are values of the derivative dH/dT_c determined by simply passing a smooth curve through our measured T_c values and through the point $(T_{\text{poly}}, H_{\text{poly}}) = (0.82 \text{ mK}, 3.90 \text{ kOe})$. This temperature assignment for T_{poly} is based on the work of Osheroff[31] and also Tang *et al.*,[30] with their respective temperature scales normalized to give 0.93 mK for $T_N(0)$. Values for dH/dT_c can also be extracted from Eqs. (33) and (34), which describe the temperature dependence of the magnetization, if $M(0,H)$ is taken from other experiments. The open circles in Fig. 24 result from using the zero-temperature magnetization data of Osheroff, Godfrin, and Ruel. The huge discrepancy between the two different determinations of the derivative, for fields near 4 kOe, are reduced if T_{poly} is allowed to increase. We comment here that Osheroff[31] used NMR resonance shifts in the LFP to measure temperatures relative to $T_N(0)$. It is possible that these temperatures are in error.[40] A higher value for T_{poly} is also in line with the results of Prewitt and Goodkind[33] and Sawada *et al.*[25]

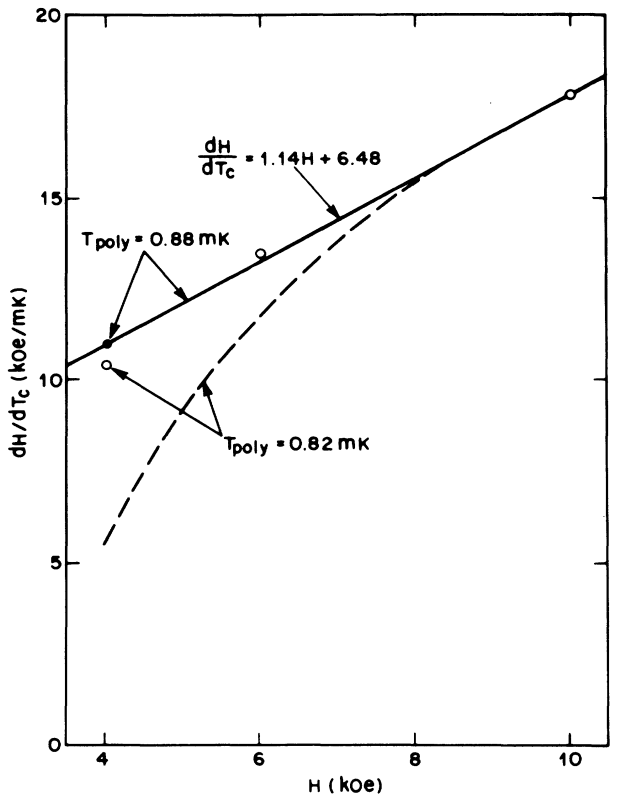

FIG. 24. Slope of the HFP-PP transition line. The dashed curve is based on the transition line determined by the new T_c values at 6 and 10 kOe and on $T_{\text{poly}} = 0.82$ mK from previous experiments. The circles are values of dH/dT_c determined by comparing the directly measured zero-temperature magnetization from Ref. 34 with that implied by Eqs. (33) and (34). Consistency between the two methods for determining the slope is obtained if T_{poly} is taken to be 0.88 mK.

Our analysis repeated using $T_{\text{poly}} = 0.88$ mK results in the solid straight line passing through the points at 6 and 10 kOe and the revised point (solid circle) at 4 kOe. The simple field dependence for dH/dT_c leads directly to

$$T_c = 0.876 \ln(0.286H + 1.62) , \tag{39}$$

with H measured in kOe and T_c in mK. Equation (39) gives T_c values which agree with our measured temperatures to within 1% and leads, via Eqs. (33) and (34), to value of $M(0,H)$ which agree with those of Ref. 34 also to within 1%. We note that Eq. (39) continues to provide a good description of T_c data[25,37] at fields up to 80 kOe.

3. T_N versus H

Here we determine $T_N(H)$ in a self-consistent manner by applying the Clausius-Clapeyron equation [Eq. (36)] to the existing set of thermodynamic data, under the constraints that $T_N(0) = 0.93$ mK and $T_N(3.90 \text{ kOe}) = 0.88$ mK. The second constraint is needed, in part, to compensate for the scarcity of precise thermodynamic data in the LFP for $H > 0$, but also to guarantee consistency with the analysis of the preceding subsection.

To proceed with the calculation we write

$$\frac{C}{R} = b(H) \left[\frac{T}{T_N(0)} \right]^3 . \tag{40}$$

The T^3 dependence for the specific heat at nonzero fields is consistent with the LFP findings of Tang *et al.* at 2.66 kOe and with the findings of Osheroff *et al.*[34] at 4 kOe. We are forced to assume next that the field-dependent amplitude can be described reasonably well by a function of the form

$$b(H) = b_0 + b_1 H^{\gamma} , \tag{41}$$

where γ is an integer.

These equations imply that

$$\frac{S}{R} = \frac{b(H)}{3} \left[\frac{T}{T_N(0)} \right]^3 , \tag{42}$$

and that

$$M(T) - M(0) = \frac{R\gamma b_1}{12} \frac{T^4}{T_N(0)^3} H^{\gamma - 1} . \tag{43}$$

Note that b_1 is expected to be positive for an antiferromagnet. A positive b_1 means that S increases with H at fixed temperature or, equivalently, that M increases with T at fixed field, i.e., an increasing temperature and/or field weakens the antiferromagnetic order. Equation (43) implies immediately that $\gamma \neq 1$, since $\gamma = 1$ leads to a nonzero magnetization even for $H = 0$. Taking $\gamma = 2$ is also ruled out since this value implies field independence for M/H, which contradicts the work of Prewitt and Goodkind. Qualitative agreement with their measurements is obtained, however, with $\gamma = 3$, Sec. III C, and so we adopt this value.

The iterative procedure for obtaining both b_1 and T_N versus H was as follows: First, T_N versus H was simply taken to be given by the straight line joining the (T,H) coordinates (0.93 mK, 0) and (0.88 mK, 3.90 kOe). For a given b_1, the quantities ΔS, ΔM, and, via the Clausius-Clapeyron equation, dT_N/dH were determined at equally spaced values of H. The derivative values were then integrated to obtain $T_N(H)$. Adjustments were made in b_1 until T_N (3.90 kOe) was equal to 0.88 mK. These results for T_N versus H were then used as a starting point for the next iteration. After three iterations the input and output temperatures, at all values of H, agreed to within better than 1 part in 10^4, for $b_1 = 0.003\,17$. Figure 25 shows the final results for $\Delta S/R$, $\Delta M/M_{\rm sat}$, and dT_N/dH plotted versus the field. The very sharp field dependence for $H \gtrsim 3.5$ kOe is a consequence of the proximity of the T_c transition line. A listing of $T_N(H)$ values is given in Table II.

It should be noted that the determination of b_1 from this analysis is very sensitive to the temperature assigned to the polycritical point. A smaller value of $T_{\rm poly}$ implies a smaller value of b_1; for $T_{\rm poly} \approx 0.83$ mK, $b_1 = 0$.

TABLE II. H-T coordinates for the boundary between the LFP and PP, and for the boundary between the LFP and HFP. These values are based on the thermodynamic analysis discussed in Sec. III D.

T_N (mK)	H (kOe)	T_{lh} (mK)	H (kOe)
0.880	3.90	0.10	4.500
0.893	3.50	0.20	4.499
0.901	3.00	0.30	4.497
0.909	2.50	0.40	4.491
0.915	2.00	0.50	4.477
0.921	1.50	0.60	4.449
0.926	1.00	0.70	4.390
0.929	0.50	0.80	4.241
0.930	0.00	0.88	3.900

4. H_{lh} versus T

The general scheme followed in determining the LFP-HFP transition line is similar to that described in the preceding subsection for $T_N(H)$. However, here there were no adjustable parameters and therefore no guarantees that the inferred transition line would be consistent with the remainder of the phase diagram. This then provided an important thermodynamic check on the empirical equations describing the specific level in both the low- and high-field phases.

Coordinates of the LFP-HFP transition line are given in Table II. Use of these in evaluating ΔS, ΔM, and dH_{lh}/dT, see Fig. 26, led, by integration, to output values of H_{lh} which agreed with the input values to

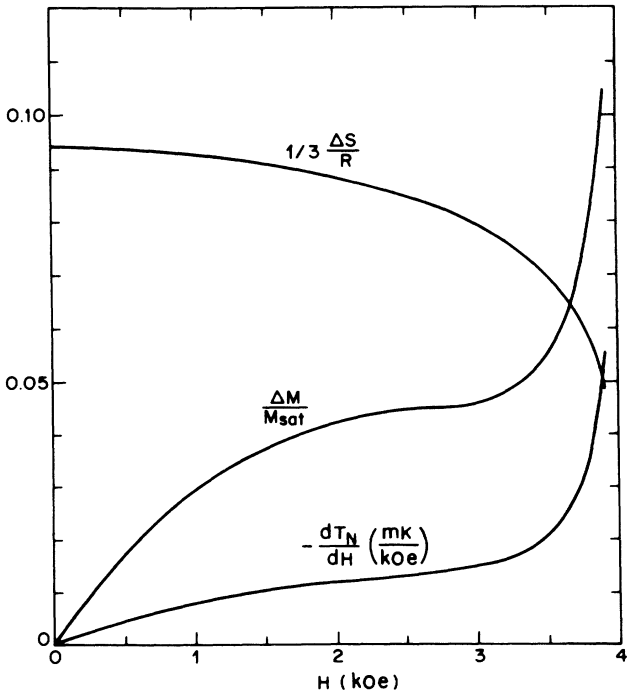

FIG. 25. First-order jumps in the entropy and magnetization at T_N, and the implied derivative dT_N/dH.

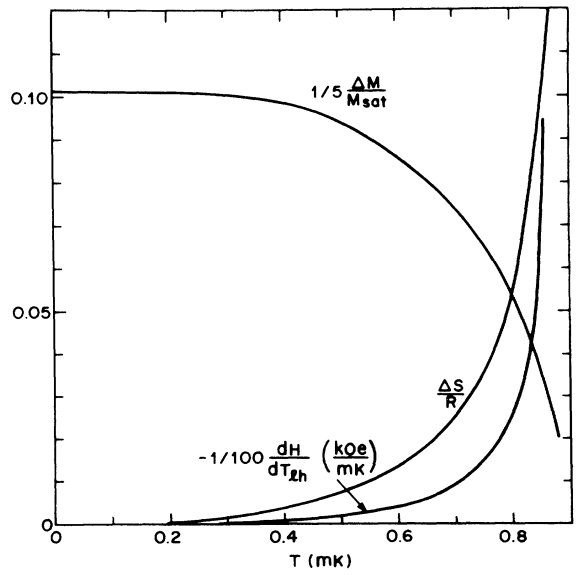

FIG. 26. First-order jumps in the entropy and magnetization at H_{lh} and the implied derivative dH/dT_{lh}.

within better than 0.3% for $T<0.8$ mK. At $T=T_{\text{poly}}$ the self-consistency in H_{lh} was 2.5%. Bearing in mind the uncertainties in the empirical equations describing the thermodynamic results, especially in the vicinity of the polycritical point, the results are satisfactory. Repeating the analysis with $b_1\equiv 0$ led to inconsistencies in H_{lh} that were an order of magnitude larger for temperatures near T_{poly}.

ACKNOWLEDGMENTS

We are grateful to R. N. Bhatt, M. C. Cross, D. S. Fisher, H. Godfrin, and D. D. Osheroff for helpful discussions, and to D. D. Osheroff, H. Godfrin, and R. R. Ruel for allowing us to use their preliminary magnetization data.

APPENDIX: THERMAL RELAXATION TIMES AND BOUNDARY RESISTANCE

As a consequence of the thermal resistance, there was a significant difference between the temperature of the cell body (i.e., the temperature measured with the LCMN thermometer) and that of the ^{3}He sample when heat was being applied to the calorimeter. This difference slowly relaxed away after the termination of the heat pulse. As indicated in Fig. 2, the size of the temperature overshoot and also the time needed to reestablish thermal equilibrium increased with increasing magnetic field. In Fig. 27 the thermal time constants, extracted from the relaxation curves near equilibrium conditions, are plotted as a function of temperature for fields of 0, 1, and 6 kOe. Other data obtained at 2, 4, and 10 kOe coincided with the 6-kOe curve; i.e., there was no detectable increase in the time constants for fields greater than 2 kOe. For temperatures greater than roughly 8 mK the heat pulses did not cause a temperature overshoot; instead, the measured temperature slowly increased toward the equilibrium value. This change in response occurred when the relaxation time became comparable to the thermometer time constant. At lower temperatures the thermometer time constant was much smaller than the thermal equilibrium times.

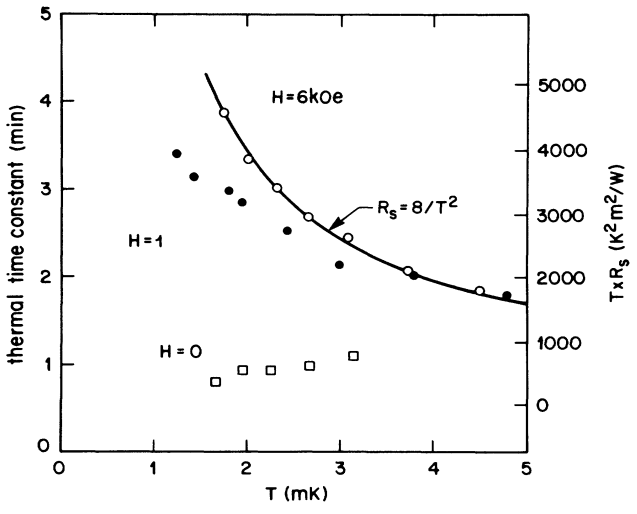

FIG. 27. Time constant associated with the reestablishment of thermal equilibrium following a heat pulse into the calorimeter. The scale on the right gives the implied boundary resistance between solid ^{3}He and silver powder.

In the vicinity of the specific-heat peak there were dramatic changes in the $H=0$ recovery times. On either side of the peak, where the specific heat was changing rapidly with temperature, the recovery times were 4 or 5 times larger than might have been anticipated from the higher-temperature data and could not be described by a single relaxation time. At the peak the times were about 1 min. Presumably, the anomalous behavior near the transition is associated with the fact that the transition is first order and also with the nonuniformity of the sample density. In the following only time-constant data obtained well above T_N are considered.

The assumption is made that the spin-lattice relaxation time is extremely short for our sample contained within the small pores of the silver sponge. The internal time constant should then be governed by the thermal diffusivity. It is estimated that this time is roughly 15 sec at 1 mK and decreasing rapidly with increasing temperature. The much longer thermal relaxation times observed are thus associated with the thermal boundary resistance.

The measured times correspond to the thermal mass provided by the liquid ^{3}He in the thermometer chamber coming into equilibrium with the thermally-more-massive solid ^{3}He sample. The main impedances occur at the liquid-^{3}He–to–silver boundary in the thermometer with resistance R_l and at the solid-^{3}He–to–silver boundary in the cell with resistance R_s. Since the heat capacity of the liquid, c_l, is small compared to that of the solid, the relaxation time is given approximately by

$$\tau=c_l(R_l/A_l+R_s/A_s)\ , \tag{A1}$$

where A_l is the surface area of the silver sinter in the thermometer (3.8 m^2) and A_s is the area in the cell (10.5 m^2). Using $c_l=2.78nRT\approx 0.460T$ J/K^2 (Ref. 12) and $R_l=(250/T)\,\text{K}^2\,\text{m}^2/\text{W}$,[41]

$$c_lR_l/A_l=30\text{ s}\ . \tag{A2}$$

Therefore,

$$R_s=\frac{A_s}{c_l}(\tau-30)=\frac{23}{T}(\tau-30)\ . \tag{A3}$$

At $H=0$, τ is nearly temperature independent and equal to 60 s (Fig. 27). We thus find $R_s\approx(690/T)\,\text{K}^2\,\text{m}^2/\text{W}$ ($V=24.13$ cm^3/mole). The scale along the right-hand side of Fig. 27 gives TR_s determined using Eq. (A3). For fields greater than 2 kOe the boundary resistance is described well by $R_s=(8/T^2)\,\text{K}^2\,\text{m}^2/\text{W}$.

It is interesting that very recently Osheroff and Richardson[42] found very similar results for the boundary resistance between *liquid* ^{3}He and silver powder from measurements covering the same temperature regime; they found $R_l\propto 1/T$ in zero field, $R_l\propto 1/T^2$ for nonzero

fields, and essentially no field dependence for $H \gtrsim 2$ kOe. Although the magnitude of our R_s is roughly a factor of 3 larger than their R_l, the true values might agree more closely. Certainly a good portion of the difference might be attributed to our correction for the boundary resistance in the LCMN thermometer and to our estimates of the surface areas. It should also be noted that Osheroff and Richardson observed R_l to increase somewhat with applied pressure. Certainly the overall agreement strongly suggests that the interfaces in the two experiments are very similar, which is consistent with there being several layers of solid helium on the silver surfaces even though the bulk of the sample is liquid.

The large boundary resistance makes it difficult to cool solid helium samples at very low temperatures and in large fields. Using the expression $R_s C_s n/A$, the time constant for cooling is estimated to be roughly 4 h at 1 mK. This value is based on $C_s \approx 0.1R$, $n = 0.02$ mole, and $A = 10.5$ m^2. Here, R is the gas constant. The time needed to remove the latent heat nL is given by $nLR_s/\Delta T\, A$. Using $\Delta S \approx 0.4R \ln 2$ and $\Delta T = 0.5$ mK leads to a time of about 20 h. It should be noted that both of these times depend on the ratio n/A and thus do not change with the size of the cell. Shorter times can be achieved by reducing n/A, but this would increase the fraction of ^{3}He surface atoms, which might behave very differently from those in the interior. A substantial reduction of these times would then seem possible only if the thermal boundary resistance could somehow be reduced.

[1]M. Roger, J. H. Hetherington, and J. M. Delrieu, Rev. Mod. Phys. **55**, 1 (1983).

[2]M. C. Cross and D. S. Fisher, Rev. Mod. Phys. **57**, 881 (1985).

[3]W. P. Halperin, F. B. Rasmussen, C. N. Archie, and R. C. Richardson, J. Low Temp. Phys. **31**, 617 (1978).

[4]R. B. Kummer, R. M. Mueller, and E. D. Adams, J. Low Temp. Phys. **27**, 319 (1977).

[5]D. S. Greywall, Phys. Rev. B **31**, 2675 (1985).

[6]Vacuum Metallurgical Co., Tokyo, Japan, 400-Å powder.

[7]P. A. Busch, S. P. Cheston, and D. S. Greywall, Cryogenics **24**, 445 (1984).

[8]R. J. Robertson, F. Guillon, and J. P. Harrison, Can. J. Phys. **61**, 164 (1983).

[9]K. A. Muething, D. O. Edwards, J. D. Feder, W. J. Gully, and H. N. Scholz, Rev. Sci. Instrum. **53**, 485 (1982).

[10]U. E. Israelsson and C. M. Gould, Rev. Sci. Instrum. **55**, 1143 (1984).

[11]P. Busch (unpublished).

[12]D. S. Greywall, Phys. Rev. B **33**, 7520 (1986).

[13]J. H. Colwell, W. E. Fogle, and R. J. Soulen, Jr., in *Proceedings of the 17th International Conference on Low Temperature Physics,* edited by U. Eckern, A. Schmid, W. Weber, and H. Wühl (North-Holland, Amsterdam, 1984), Pt. 1, p. 395; and private communication.

[14]D. S. Greywall and P. A. Busch, J. Low Temp. Phys. **46**, 451 (1982).

[15]T. Haavasoja, Ph.D. thesis, Helsinki University of Technology, 1980 (unpublished); T. A. Alvesalo, T. Haavasoja, and M. T. Manninen, J. Low Temp. Phys. **45**, 373 (1981); T. A. Alvesalo, T. Haavasoja, M. T. Manninen, and A. T. Soinne, Phys. Rev. Lett. **44**, 1076 (1980).

[16]D. D. Osheroff, M. C. Cross, and D. S. Fisher, Phys. Rev. Lett. **44**, 792 (1980).

[17]A. K. McMahan (unpublished).

[18]W. P. Halperin, Ph.D. thesis, Cornell University, 1975 (unpublished).

[19]R. A. Guyer, J. Low Temp. Phys. **30**, 1 (1978).

[20]D. S. Greywall, Phys. Rev. B **15**, 2604 (1977); **16**, 5129(E) (1977).

[21]G. A. Baker, H. E. Gilbert, J. Eve, and G. D. Rushbrooke, Phys. Rev. **164**, 800 (1967).

[22]W. P. Kirk and E. D. Adams, Phys. Rev. Lett. **27**, 392 (1971).

[23]E. Suandeau, M. Roger, and M. E. R. Bernier (unpublished).

[24]J. M. Dundon and J. M. Goodkind, Phys. Rev. Lett. **32**, 1343 (1974).

[25]A. Sawada, H. Yano, M. Kato, K. Iwahashi, and Y. Masuda, Phys. Rev. Lett. **56**, 1587 (1986).

[26]H. L. Stipdonk and J. H. Hetherington, Phys. Rev. B **31**, 4684 (1985).

[27]M. C. Cross and R. N. Bhatt, J. Low Temp. Phys. **57**, 573 (1984).

[28]D. D. Osheroff and C. Yu, Phys. Lett. **77A**, 458 (1980).

[29]T. Hata, S. Yamasaki, M. Taneda, T. Kodama, and T. Shigi, Phys. Rev. Lett. **51**, 1573 (1983).

[30]Y. H. Tang, E. D. Adams, and K. Uhlig, Phys. Rev. Lett. **57**, 222 (1986).

[31]D. D. Osheroff, Physica **109&110B**, 1461 (1982).

[32]K. Uhlig, E. D. Adams, G. E. Haas, R. Rosenbaum, Y. Morii, and S. F. Kral, in *Proceedings of the 17th International Conference on Low Temperature Physics,* Ref. 13, Pt. 1, p. 279.

[33]T. C. Prewitt and J. M. Goodkind, Phys. Rev. Lett. **44**, 1699 (1980).

[34]D. D. Osheroff, H. Godfrin, and R. R. Ruel, Phys. Rev. Lett. **58**, 2458 (1987).

[35]D. D. Osheroff and P. W. Anderson, Phys. Rev. Lett. **33**, 686 (1974).

[36]H. Godfrin, Ph.D. thesis, University of Grenoble, 1981 (unpublished).

[37]H. Godfrin, G. Frossatti, A. S. Greenberg, B. Hebral, and D. Thoulouze, Phys. Rev. Lett. **44**, 1695 (1980).

[38]E. D. Adams, E. A. Schubert, G. E. Haas, and D. M. Bakalyar, Phys. Rev. Lett. **44**, 789 (1980).

[39]E. D. Adams, K. Uhlig, Y. H. Tang, and G. E. Haas, Phys. Rev. Lett. **52**, 2249 (1984).

[40]D. D. Osheroff (private communication).

[41]K. Andres and W. O. Sprenger, in *Proceedings of the LT-14 (Otaniemi, Finland),* edited by M. Krusius and M. Vuorio (North-Holland, Amsterdam, 1975), Vol. 1, p. 123.

[42]D. D. Osheroff and R. C. Richardson, Phys. Rev. Lett. **54**, 1178 (1985).